Chemical Science

EDGE ARTICLE

View Article Online
View Journal | View Issue

Direct monitoring of protein–protein inhibition using nano electrospray ionization mass spectrometry†

Cite this: *Chem. Sci.*, 2014, **5**, 2794

Dragana Cubrilovic,[a] Konstantin Barylyuk,[a] Daniela Hofmann,[b] Michal Jerzy Walczak,[b] Martin Gräber,[c] Thorsten Berg,[c] Gerhard Wider[b] and Renato Zenobi*[a]

Received 7th December 2013
Accepted 18th March 2014

DOI: 10.1039/c3sc53360c

www.rsc.org/chemicalscience

Dissociation of the TNF-alpha trimer caused by the small-molecule inhibitor SPD304 was monitored using native ESI-MS and ion mobility spectrometry (IMS). Upon addition of the inhibitor, our data clearly indicate partial dissociation of the protein into dimers and monomers. The IMS-MS analysis shows that dimeric ions have their own characteristic drift time distributions, which are different from those of the dimer ions originating in the gas phase due to collision-induced dissociation. We show that only one equivalent of the inhibitor binds to the trimeric form. We also investigated inhibition of heterodimer formation of the survival protein Bcl-x_L with the cell death-promoting regions of the proteins Bak and Bad, using the small inhibitors ABT737 and ABT263. We found that ABT737 is more potent than ABT263 in preventing the heterodimerization between Bcl-x_L and the Bak and Bad derived BH3 peptides. We could also monitor the mode of binding, which in this case is competitive. These results indicate that native ESI-MS can be widely used to study the inhibition of other relevant protein–protein interactions (PPIs), and provide a good basis for further improvement and identification of small-molecule PPI inhibitors.

Introduction

Protein–protein interactions (PPIs) are of fundamental importance in most biological processes – from intercellular function to programmed cell death.[1–3] The controlled disruption of PPIs with small-molecule inhibitors is of high interest in current drug discovery due to the large number of protein–protein interactions involved in signalling pathways related to cancer and many other human diseases. In the last decade, significant progress in the design and development of potential small inhibitors of PPIs has been made.[2,4,5] Therefore, understanding of the mechanisms of protein–protein disruptors can be used in several fields, *e.g.*, in small molecule drug discovery, in order to design and optimize novel potential therapeutics.

The conventional tools and methodologies for investigating PPIs include physicochemical methods such as X-ray crystallography, NMR spectroscopy, surface plasmon resonance (SPR), isothermal titration calorimetry (ITC), fluorescence spectroscopy, or biochemical methods. All these techniques have particular strengths and weaknesses in terms of sample consumption, throughput, dynamic range; some require immobilization of one of the binding partners.[6–10]

Another powerful and increasingly utilized method to detect and characterize noncovalent interactions is nanoelectrospray ionization mass spectrometry (nanoESI-MS).[11–13] It has been shown by many research groups that proteins in the gas phase are in a folded conformation, which is similar to the native conformation in solution, and that they are therefore able to bind inhibitors and provide a "snapshot" of the solution-phase equilibrium.[14–17] In recent years, nanoESI-MS has become increasingly used in drug discovery, for the investigation of protein–ligand and protein–protein interactions.[17–21] This technique can address key questions about composition, stoichiometry, subunit interactions, and architectural organization of noncovalent complexes.[22] The present work emphasizes the advantages of the native MS approach for direct monitoring of protein–protein inhibitions. Pioneering work in the detection of protein–protein interaction inhibition *via* ESI-MS was carried out by Grygon and co-workers.[23] Besides the quantification of protein–protein interactions it offers the possibility to directly visualize ligation states and conformational changes upon addition of small disruptor molecules in solution.

In this work we have also applied ion mobility (IM) spectrometry, which is a gas-phase separation tool comparable to electrophoresis in solution, and which can be combined with MS. This is a technique that allows ions to be separated by a weak electric field in a gas environment according to their mobility.[22] From measurements of the ion transport properties,

[a]*Department of Chemistry and Applied Biosciences, ETH Zurich, 8093 Zurich, Switzerland. E-mail: zenobi@org.chem.ethz.ch*

[b]*Department of Molecular Biology and Biophysics, ETH Zurich, 8093 Zurich, Switzerland*

[c]*Institute of Organic Chemistry, University of Leipzig, 04103 Leipzig, Germany*

† Electronic supplementary information (ESI) available. See DOI: 10.1039/c3sc53360c

ion size information can be generated. This results in an orientationally averaged ion-neutral collision cross section (CCS).[24] Recent studies show good correlation of many data sets between CCS values based on IM measurements and X-ray or NMR data sets for the same proteins and complexes in solution. Although these measurements are carried out in the absence of bulk water, these studies suggest that IM data reflect condensed phase properties and can be used as a technique for structural biology. Some of the recent reviews summarizing the developments of IM-MS to rapidly measure changes in protein structure, oligomeric state, and binding stoichiometry from complex mixtures are by Niu *et al.*,[24] Hall and Robinson,[25] and Konijnenberg *et al.*[26]

In this contribution we first investigated the alpha tumour necrosis factor (TNF-alpha), a cytokine involved in systemic inflammation and in immune regulation, and therefore a therapeutic target for many diseases. The known inhibitor SPD304 was used to induce dissociation of the trimeric TNF-alpha, as monitored by nanoESI-MS.[27] In addition we performed ion mobility mass spectrometry (IM-MS) experiments. NanoESI-MS and IM-MS results are in agreement, and, upon ligand addition, show dissociation of the trimer into dimers and monomers. The IMS-MS analysis shows that dimeric ions have their own characteristic drift time distributions, which are different from dimer ions generated in the gas phase due to CID. Therefore dissociation occurs due to SPD304-promoted dissociation of TNF-alpha trimers in solution. The mode of inhibitor binding to the TNF-alpha was studied as well.

The second system investigated in this study is the interaction between the antiapoptotic Bcl-2 family protein Bcl-x_L and two different proapoptotic binding partners, Bak and Bad. The proapoptotic is similar to the antiapoptotic group in a single alpha helix called the BH3 region, which is essential for binding to Bcl-x_L and also required for the proapoptotic effect.[28–33] Heterodimerization between members of the Bcl-2 family of proteins plays a key role in the regulation of programmed cell death. In a first step we investigated the heterodimerization between Bcl-x_L and the BH3 domain of Bak and Bad derived synthetic peptides, which bind with high affinity *in vitro*; it has also been shown that the Bak BH3 peptide alone can induce apoptosis in various cell lines.[30] Titration experiments at constant Bcl-x_L and different peptide concentrations were first performed using nanoESI-MS. Results are in agreement with these from other biophysical methods. In the second step, we investigated the recently introduced small BH3 mimetic inhibitors ABT737 and ABT263 that are designed to disrupt the above-mentioned cancer-linked protein–protein interactions. These small-molecule inhibitors have been found to occupy the BH3 binding groove of anti-apoptotic Bcl-2 family members, preventing them from antagonizing proapoptotic proteins and induce apoptosis, thereby enhancing programmed cell death of cancer.[29,34] NanoESI-based results show that ABT737 prevents the heterodimerization of Bcl-x_L·Bak as well as Bcl-x_L·Bad more efficiently compared to ABT263. We also observed competition of the small molecule inhibitors with the BH3 derived peptide for the same Bcl-x_L binding pocket, clearly indicating the mechanism of binding.

All nanoESI-MS based results obtained show that this technique is a valuable tool for investigation of PPI inhibition. In addition to the quantification of binding strengths of PPIs, we could gain information about stoichiometry, conformational changes, binding mechanism, and relative binding strengths of the small PPI inhibitors from single-point measurements. Key advantages of native MS are its simplicity (label-free measurements), selectivity (possibility of using additional stages of MS combined with ion activation methods), sensitivity (low sample consumption), and speed (mass spectra can be acquired in less than a minute).

Experimental section

Materials and methods

All solvents and caesium iodide (CsI) were purchased from Sigma Aldrich (Buchs, Switzerland). The pET29 plasmid bearing the coding sequence of Bcl-x_L (amino acids 1-209, Δ45–84) was a kind gift from Prof. Ho Sup Yoon (Nanyang Technical University, Singapore).[31] The Bcl-x_L protein expression has been previously described.[28] The expression and purification protocol of TNF-alpha (A. Corti)[35] was shortened and optimized by introduction of the N-terminal $(His)_6$-tag. This allows for use of a Ni-NTA affinity purification step that significantly shortens the entire purification protocol. Owing to the Ni-NTA step, troublesome and time-consuming hydrophobic chromatography and desalting at 65% ammonium sulphate steps can be skipped. This results in a higher yield of purified protein; the His-tag also allows immobilization of TNF on different media (*e.g.* BiaCore chip or Ni-NTA beads). The BH3 peptide domains of the Bad (NLWAAQRYGRELRRMSDK) and the Bak protein (GQVGRQLAIIGDDINR) were obtained from Genscript (NJ, USA) and Anaspec (Fremont, USA), respectively. The small-molecule inhibitor SPD304 was purchased from Cayman Chemicals (MI, USA), ABT737 and ABT263 from Selleckchem (TX, USA). Water was purified using a Milli-Q® Ultrapure water purification system (Millipore, Barnstead, USA). Prior to mass spectrometric analysis the Bcl-x_L protein stock solution (224 μM) in 50 mM Hepes, 100 mM NaCl, 10% glycerol, 1 mM EDTA, 1 mM DTT, 0.1% Nonidet-40 substitute (pH = 7.5) and the TNF-alpha protein stock solution in 50 mM phosphate buffer, 100 mM NaCl, 2.5 mM EDTA (pH = 7.7) were desalted and buffer exchanged (PD MiniTrap G-25, GE Healthcare, Buckinghamshire, UK) against the ammonium acetate buffer. The stock solutions of Bad and Bak as well as the small molecule inhibitors were dissolved in DMSO at a concentration of 10 mM and further diluted in ammonium acetate to desired concentration. All MS titration experiments were recorded under "native-like" conditions using 50 mM ammonium acetate buffer (pH = 7.7) for TNF-alpha-SPD304 and 300 mM (pH = 7.5) for Bcl-x_L-peptide–inhibitor complex. To ensure the integrity of the protein complexes we kept the pH of the ammonium acetate buffer the same as that of the buffer used for protein expression and storage, which was previously optimized. In all experiments the DMSO concentration did not exceed 1% (v/v). For TNF-alpha denaturation, ZipTip columns containing C_4-resin (Millipore, Molsheim, France) were used. The exact TNF-alpha and Bcl-x_L

concentration was determined using a UV spectrometer (Genesys 10S UV-VIS, ThermoScientific, Bremen, Germany) by measuring the absorbance at 280 nm.

Mass spectrometry

NanoESI-MS analyses were performed with a hybrid quadrupole time-of-flight mass spectrometer (Q-TOF ULTIMA, Waters/Micromass, Manchester, UK) in positive ion mode. The instrument was controlled *via* the MassLynx software (version 4.0). Sample solutions were directly infused with gold/palladium-coated borosilicate glass offline nanoESI emitters (Thermo Fisher Scientific, Reinach, Switzerland) using a commercial nanoESI ion source (Waters/Micromass, Manchester, UK). The capillary voltage was set to 1.8 kV and a gentle backing pressure of 0.3–0.5 bar was applied to assist the liquid sample flow. The source temperature was kept at room temperature. Instrumental conditions had to be adjusted in order to get narrow peaks of the detected ions without dissociating the noncovalent complex. The precise settings have an influence on the peak shape: due to adduct formation with salt and buffer molecules from the spray solution, peaks might be broadened. The mass spectrometer was run with the following gentle desolvation parameters: the cone and first ion tunnel RF1 voltages, parameters that control the kinetic energy of the ions in the source region of the mass spectrometer, were set to 50 and 50 V for Bcl-x_L; and 70 and 60 V for TNF-alpha experiments, respectively. After this stage, the ion beam passed a hexapole collision cell filled with argon (purity 5.0, PanGas, Zurich, Switzerland). The collision energy offset was used to optimize desolvation and set to 22 V. The pressure in the source was increased to 5.5 mbar, using a "speedivalve" (Edwards Ltd., Sussex, UK) connected between the rotary pump and source pumping line. All instrument parameters used (*e.g.* capillary voltage, cone voltage, RF1 voltage, collision energy) were carefully adjusted and optimized to be as soft as possible for all investigated protein complexes. Collision-induced dissociation (CID) used for TNF-alpha MS/MS experiments were performed by adjusting the acceleration collision energy (CE) offset until full dissociation of the parent ions was achieved. The ion transmission was optimized for a m/z range between 100 and 9000 Da for TNF-alpha, and 100–5000 Da for Bcl-x_L. The scan time and interscan times were 1 and 0.2 s, respectively.

IMS-MS experiments were performed on a Synapt G2-S HDMS (Waters, Manchester, UK). Ions were produced by a commercial NanoLock Spray ionization source (Waters, Manchester, UK) using offline capillary emitters (see above). A capillary voltage of 0.8–1.3 kV and a backing pressure of 0.25–0.3 bar were applied to generate the nano-electrospray. The sampling cone voltage and the source offset were set to 20 and 80 V, respectively. The traveling-wave ion guides were tuned to minimize unwanted fragmentation of ions during ion transfer, trapping, ion mobility separation, and mass analysis. For instance, the trap DC bias, helium cell DC offset, and IMS bias were lowered to 40, 30 and 0.5 V, respectively. The trap gas flow was increased to 5.5 ml min^{-1} to facilitate transmission of high-m/z ions. The trap and transfer collision energies were set to 10 and 5 V, respectively, and trap and transfer CID was induced by increasing the corresponding voltage offsets. Ion mobility separations were carried out using IMS wave velocity (WV) ramping of 1600 to 200 m s^{-1} (unless specified differently) and a wave height (WH) amplitude of 40 V. Nitrogen (purity 5.0, PanGas, Zurich, Switzerland) was used as IMS buffer gas. The spectra were acquired in the range of m/z 50–8000 using a scan time of 2 s and an interscan delay of 0.01 s. Typically, at least 50 scans were combined to produce a spectrum.

Calibration of the mass spectrometry instrument was performed using caesium iodide (CsI) clusters. CsI was dissolved in water–2-propanol (1/1, v/v) at a concentration of 2 μg μl^{-1}.

Data processing

Before data processing, each mass spectrum was smoothed (Savitzky–Gollay smooth) with the MassLynx 4.0 software (Waters, UK). For the dissociation constant (K_D) determination of the Bcl-x_L·Bad and Bcl-x_L·Bak complexes the measured relative peak heights (I) were used. The peak height ratio (R) of the Bad- and Bak-bound Bcl-x_L complex (P·L) to bare protein (P), $R = I(\mathrm{P\cdot L})/I(\mathrm{P})$, was calculated for each spectrum. For this determination, all charge states were taken into account. The ratio of the sum of all detected complex species divided by the sum of the free protein was determined. The experimentally calculated relative peak heights were plotted *versus* the total added Bad or Bak concentration. The equation derived by Daniel *et al.*[12] was used to determine the K_D values from fitting a titration curve:

$$\frac{I(\mathrm{P\cdot L})}{I(\mathrm{P})} = \frac{1}{2}\left(-1 - \frac{[\mathrm{P}]_0}{K_D} + \frac{[\mathrm{L}]_0}{K_D} + \sqrt{4\frac{[\mathrm{L}]_0}{K_D} + \left(\frac{[\mathrm{L}]_0}{K_D} - \frac{[\mathrm{P}]_0}{K_D} - 1\right)^2}\right)$$

The K_D calculations and the fitting of the titration curves were performed using the MATLAB software (2010a, The MathWorks, Natick, MA, USA).

Results and discussion

NanoESI-MS analysis of TNF-alpha

Prior to the addition of the inhibitor to TNF-alpha, the proper instrumental conditions had to be adjusted to preserve the trimeric protein structure. Therefore trimeric human TNF-alpha was analysed under denaturing and "native" conditions using Q-TOF ULTIMA. In Fig. S1 (ESI),† nanoESI mass spectra for a solution of denatured and native TNF-alpha are shown. The first spectrum measured under denatured conditions generates a broad charge state distribution. Under this condition the completely unfolded monomer that appears in the lower m/z range is detected. In contrast, Fig. S1B† displays the spectrum under "native-like" conditions in 50 mM ammonium acetate and 1% DMSO at pH = 7.7. The observed narrow charge state distribution, predominantly +11, +12, +13, is typical for non-denaturing conditions, and is consistent with a compact conformation in solution. In addition to the trimeric TNF-alpha ions, we can observe minor monomeric peaks at +7, +6, as well.

Many studies have demonstrated that the charge state distribution depends on the protein conformation in solution.[36–38] Native nanoESI-MS analysis of the protein is relevant, since proper TNF-alpha folding is crucial for the later interaction with the inhibitor in solution.

In addition we performed CID experiments in order to confirm the trimeric TNF-alpha assembly and gain additional information about the protein stability in the gas phase. For the MS/MS measurements the +14 trimeric ions were selected and dissociated during transmission through the mass spectrometer. For this, the CE offset was varied in 10 V steps from 15 to 100 V, until the selected trimeric ions were completely dissociated. In Fig. S2† two different CID spectra at a CE offset of 30 and 100 V are shown. Dissociation of the precursor ions yielded the dimeric and monomeric protein ions. These CID experiments provide additional evidence for the trimeric TNF-alpha assembly. In should be mentioned that different charge state distributions are generated in the absence and in the presence of 1% DMSO. This effect is described in the next subsection in more detail.

Monitoring the disruption of the TNF-alpha trimer due to the binding of the inhibitor SPD304 by nanoESI-MS and ion mobility-MS

SPD304 has previously been identified as a potent inhibitor of TNF-alpha. We monitored the influence of SPD304 on TNF-alpha using nanoESI- and ion mobility-MS. At this point it is worth noting that the described experiments were run in 1% DMSO (v/v). It has been shown that this amount of DMSO will not significantly influence the binding of the small molecule to the protein as observed by nanoESI-MS.[39] However, it is still necessary to perform experiments in the presence and in the absence of DMSO. This should be considered in order to properly evaluate any possible conformational difference, resulting in a different charge state distribution, of the complex and the bare or dissociated protein. Also, DMSO may lead to partial dissociation of the protein. Fig. 1 illustrates IMS-MS analysis of TNF-alpha under "native ESI-MS" conditions. The results shown should provide additional structural information based on the separation of gas-phase ions based on their differential transport through an environment of an inert neutral gas.[24] We show the 2D IMS drift time *vs.* *m*/*z* plots with corresponding mass spectra and drift time distributions. We first performed experiments using a 4.5 μM TNF-alpha solution in 75 mM ammonium acetate buffer at pH = 7.7 and the same protein concentration in the presence of 1% (vol.) DMSO. In the presence of 1% DMSO, an overall charge state reduction can be observed; +11, +12, +13 compared to +13, +14, +15, +16. The appearance of a small amount of the monomers is also observed in the presence of DMSO. The trimeric form is compact in both cases. In our next experiment, we investigated the influence of the inhibitor by adding 100 μM SPD304 to 4.5 μM trimeric TNF-alpha in 75 mM ammonium acetate solution at pH = 7.7 in 1% DMSO. The same charge state distribution is detected for TNF-alpha upon inhibitor addition. Again, three different compact charge states representing the TNF-alpha trimer are observed.

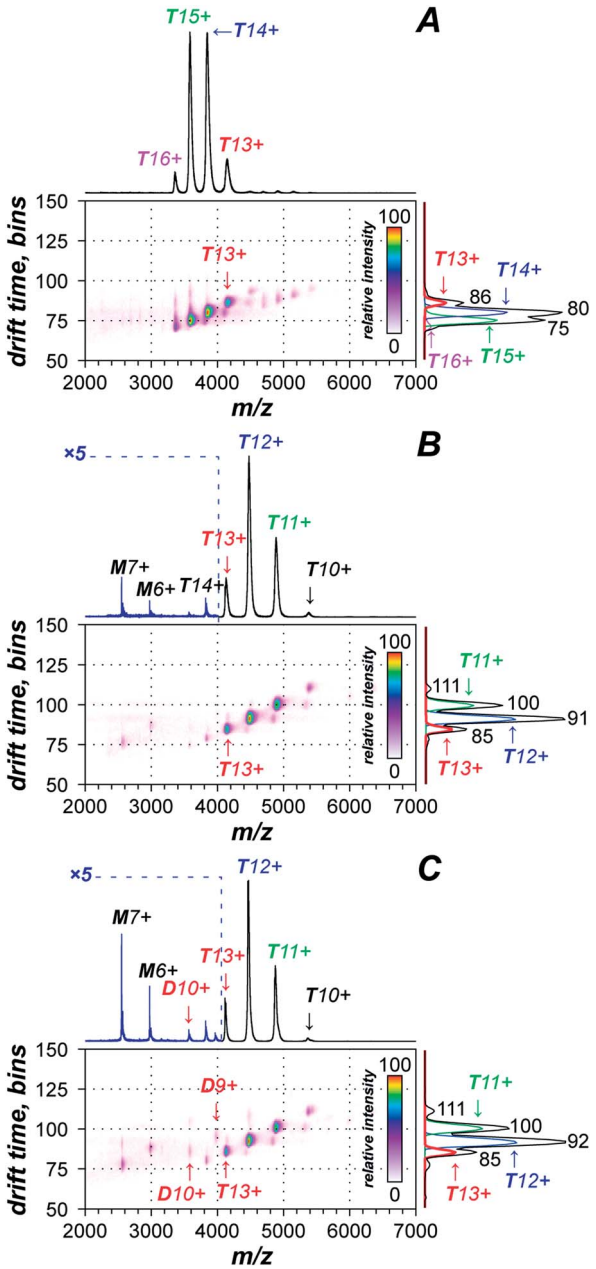

Fig. 1 IMS-MS analysis of TNF-alpha under native ESI-MS conditions. Shown are plots of 2D IMS drift time *vs.* *m*/*z* with corresponding mass spectra (top traces) and drift time distributions (traces on the right). Peaks corresponding to monomeric, dimeric, and trimeric TNF-alpha ions are labelled as M, D, and T, respectively, and their charge states are indicated. Peak maxima in the drift time distributions are labelled with the respective bin numbers. Along with the integral drift time distributions (black traces), some selected-ion drift time distributions are shown in color. Peak labels are color-coded accordingly. (A) 4.5 μM TNF-alpha solution in 75 mM ammonium acetate buffer pH 7.7. (B) Same as in (A), but in the presence of 1% (vol.) DMSO: note the overall charge state reduction and the appearance of a small amount of monomers. (C) Same as in (A), but in the presence of 1% (vol.) DMSO and 100 μM SPD304: note the appearance of dimer ions and the increase of monomer peak intensities. Parts of the mass spectra in (B and C) are shown at 5-fold magnification.

The appearance of dimer ions and the increase of monomer peak intensities is clearly seen, indicating the dissociation of the trimeric protein form in solution. The advantage of IM-MS in this case is the clear separation of dimer and trimer ions due to their different drift times.

The peak maxima in the drift time distributions are represented with the respective bin numbers. As can been seen in Fig. 1, the +13 charge state of the trimeric protein appears in all three cases (without DMSO, with DMSO, and upon ligand binding). The +13 charge state shows the same drift time distribution in all three cases. These results indicate clearly that the dissociation upon ligand addition happens in solution and is not due to partial dissociation of the trimer in the gas phase.

Under this aspect, we have also investigated the dependence of the drift time distribution of the TNF-alpha trimer 13+ ion on the trap collision energy applied (Fig. S3†). This charge state was chosen since it is generated in all three cases (with and without DMSO and in the presence of the inhibitor). The selected 13+ ions were interrogated by changing the trap collision voltage in the ion trap just prior to the mobility cell. The increased voltage accelerates the ions such that they encounter neutral gas molecules with greater kinetic energy in the ion trap. Nearly identical collision-induced unfolding profiles registered for the TNF-alpha T13+ ion electrosprayed from various solution conditions (buffer, 1% DMSO, 1% DMSO + 100 μM ligand) is observed. The drift time distribution of the T13+ ion is narrow and unimodal in all three cases, with the peak maximum in bins 85–86 up to a trap collision energy offset of 30 V. At a collision energy of 40 V, unfolding starts, which is manifested by a slight broadening of the drift time distribution and a minor shift of the peak towards shorter drift time, due perhaps to a gas-phase collapse of the trimer. As the collision energy increases to 50 and 60 V, the drift time distribution broadens dramatically, shifts towards higher drift times, and becomes multimodal, with several more or less overlapping peaks. Dissociation into monomer and dimer ions with asymmetric charge partitioning is observed simultaneously in the mass spectrum (data not shown). At high trap collision energies, the drift time distribution coalesces into a single peak at bin 108. This behavior resembles a two-state, all-or-none protein-unfolding behavior.[40–42] The most important conclusion is that the behavior of T13+ is the same in all three cases, *i.e.*, that there are no stabilizing or de-stabilizing effects found in the gas phase when the protein is incubated with DMSO or ligand.

In Fig. 2, the IMS-MS analysis of the TNF-alpha ions produced under "native ESI" conditions from 4.5 μM protein solution in 75 mM ammonium acetate buffer (pH 7.7) containing 1% (vol.) DMSO and 100 μM SPD304 is shown. The sample was analysed at various transfer collision energy offsets. The ions were interrogated by changing the transfer collision voltage in the transfer region just after the mobility cell. TNF-alpha dimer ions D8+, D9+, and D10+ are present even at low transfer collision energy offsets (Fig. 2A and B). At high collision energy offsets (Fig. 2C and D), collision-induced dissociation (CID) of TNF-alpha ions occurred in the transfer region of the mass spectrometer, after IMS separation. Thus, fragment ions have the same drift time, as the respective parent. The D8+, D9+, and D10+ ions have their own characteristic drift time distributions, which are different from those of the dimer ions originating in the gas phase due to CID. Therefore, D8+, D9+, and D10+ ions must have been present in the sample prior to IMS-MS analysis, *i.e.* they occurred due to SPD304-promoted dissociation of TNF-alpha trimers in solution.

In addition, we have performed nanoESI-MS measurements on the Q-TOF ULTIMA. Fig. S4† shows the influence of adding 100 μM SPD304 to 4.5 μM trimeric TNF-alpha on the nanoESI mass spectra in 50 mM ammonium acetate solution at pH = 7.7 in 1% DMSO. Interestingly, here we can observe a wider charge state distribution in the spectrum compared to the above-mentioned results. Additional charge states, the +14, +15 and +16 ions, are generated compared to the spectrum without inhibitor (see Fig. S1B†). However, it would be quite speculative to state that this shift in charge state distribution towards lower *m*/*z* indicates a "less compact" trimeric protein structure in the presence of SPD304. This "more open" trimeric form may go hand in hand with a partial dissociation of the protein into dimers and monomers, which indicates a conformational change in the protein structure. The observation that the dimer abundance is lower compared to monomers is probably due to a lower ionization efficiency of the dimeric form. A very interesting result is that TNF-alpha forms a noncovalent complex by binding one inhibitor molecule. No ligation states with two or three ligands were detected.

A X-ray structure reveals that a one equivalent of the inhibitor molecule displaces a subunit of the trimer and leads to the formation of a dimeric protein form. Biophysical experiments as well as biochemical and cell-based assays have shown that the inhibitor was capable of dissociating the TNF-alpha trimer in solution and also the interaction between intact trimeric protein, which lead to subunit dissociation.[27] The ESI-MS and IM-MS results are in agreement with this structural data, but complement them in the sense that we gain additional insight into inhibitor binding to TNF-alpha.

K_D determination of the Bcl-x_L·Bak and Bcl-x_L·Bad complexes by the nanoESI-MS titration method

As a second system we investigated the heterodimerization between members of the Bcl-2 family of proteins, which is very important in regulating programmed cell death. The subsequent influence of small molecule disruptors on these interactions was monitored as well. In the first step, before addition of small disruptors ABT737 and ABT263, we carried out measurements with Bcl-x_L (amino acids 1–209, Δ45–84) in complex with the synthetic peptides of the Bak- and Bad BH3 domain. In Fig. 3A the nanoESI mass spectra of the bare protein in the presence and in the absence of Bak in 300 mM aqueous ammonium acetate at pH = 7.5 are shown. A narrow charge state distribution, predominantly 7+, 8+ ions, appears at fairly high *m*/*z*. This is characteristic for native conditions, and consistent with a compact conformation of Bcl-x_L in solution. In order to determine the dissociation constant *via* the titration method, a set of nanoESI experiments was performed with

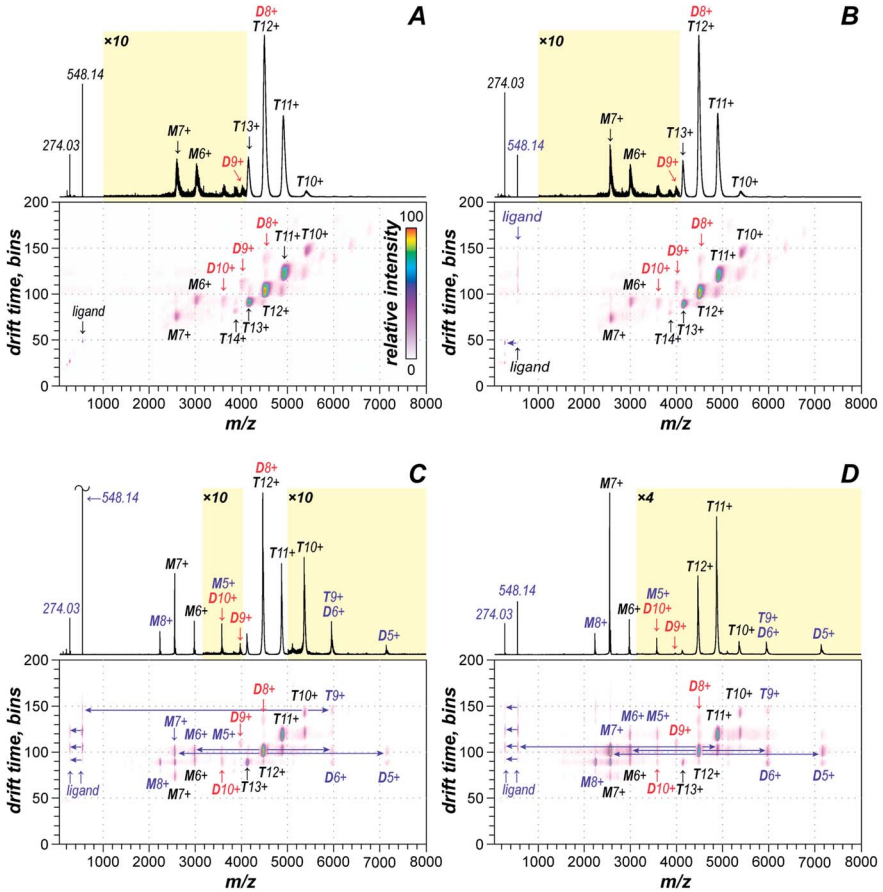

Fig. 2 IMS-MS analysis of TNF-alpha ions produced under "native ESI" conditions from 4.5 μM protein solution in 75 mM ammonium acetate buffer (pH 7.7) containing 1% (vol.) DMSO and 100 μM SPD304 (marked as ligand). The samples were analyzed at various transfer collision energy offsets: 5 V (A), 30 V (B), 90 V (C), and 130 V (D). Peaks corresponding to monomeric, dimeric, and trimeric TNF-alpha ions are marked as M, D, and T, respectively, and their charge states are assigned. Note the presence of TNF-alpha dimer ions D8+, D9+, and D10+ (marked in red) even at low transfer collision energy offsets (A and B). At high collision energy offsets (C and D), collision-induced dissociation (CID) of TNF-alpha ions occurred in the transfer region of the mass spectrometer, after IMS separation (fragments marked with blue text). Thus, fragment ions have the same drift time, as the respective parent ions (some dissociation channels are indicated with blue arrows). Note that D8+, D9+, and D10+ ions have their own characteristic drift time distributions, which are different from those of the dimer ions originating in the gas phase due to CID. Therefore, D8+, D9+, and D10+ ions must have been present in the sample prior to IMS-MS analysis, *i.e.* they occurred due to SPD304-promoted dissociation of TNF-alpha trimers in solution.

increasing Bak concentrations ranging from 0.5 to 3 μM, at a constant Bcl-x_L concentration. Fig. 3A displays representative nanoESI spectra obtained for the Bcl-x_L·Bak complex at three different ligand concentrations. As expected, increased complex signal intensity was observed with higher total Bak concentration. At 3 μM Bak concentration, full complexation was reached (data not shown). Titration experiments for Bcl-x_L·Bak binding over a range of concentrations were performed. We can detect different complex/free protein ratios for different charge states. This phenomenon is well known and has already been mentioned for different noncovalent complexes, although no clear explanation can be found in the literature.[6,22,43] In order to determine the K_D we took the abundance (peak intensities) of all detected complex and protein ions into account. The titration curve is shown in Fig. 3B. The signal ratio of the detected complex and the sum of the free protein and the complex signal was plotted against the total ligand concentration (L_0). The K_D determined by a set of titration experiments was 314 ± 35 nM. This value is in very good agreement with other values determined for Bcl-x_L·Bak in solution. In the literature, K_D values of 480 nM and 340 nM using a fluorescence polarization-based competition assay were obtained.[31,32]

For Bcl-x_L in complex with the Bad BH3 derived peptide we performed titration experiments as well. The charge state distribution is comparable with that obtained for Bcl-x_L·Bak. However, higher Bad concentrations were needed to reach full complexation. Therefore the titration experiments were performed from 2 to 20 μM (data not shown). The K_D determined for Bad binding to BcL-x_L is 4.45 ± 0.3 μM. Depending on the length of the synthetic Bad peptide K_D values ranging from 50 μM to the low nanomolar range were found using a fluorescence polarization competition assay.[44]

For the Bcl-x_L·Bak and Bcl-x_L·Bad disruption with ABT737 and ABT263, we performed the experiments at concentrations

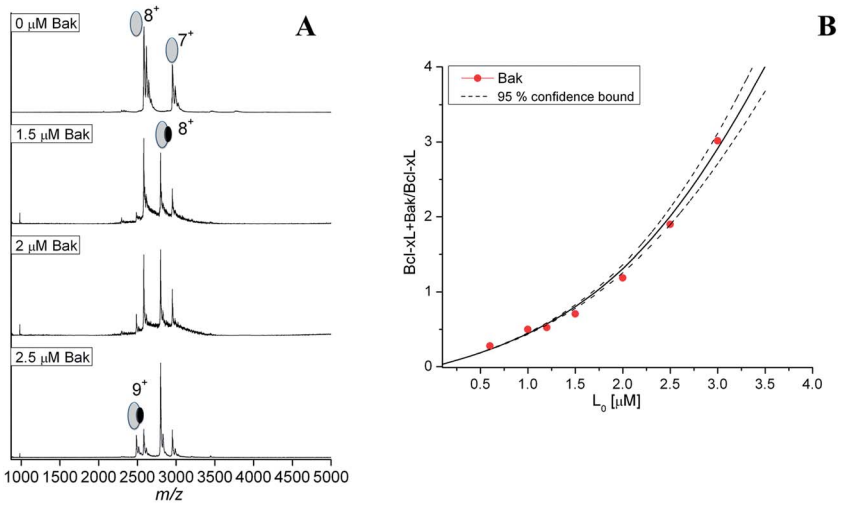

Fig. 3 (A) Representative nanoESI mass spectra of 3 μM Bcl-x_L in complex with Bak (filled circle) obtained in positive ion mode under "native" conditions. In the first spectrum adduct formation due to the small residue of HEPES buffer is detected. Titration experiments are shown adding different Bak concentrations to the Bcl-x_L. The signal for the noncovalent complex clearly increases with increasing Bak concentration present in solution. (B) NanoESI-MS titration curves for the Bcl-x_L·Bak complex. The Bak concentration ranges from 0.5 to 3 μM, while the protein concentration was kept constant.

where mainly the complex peak is observed in the spectrum. In case of Bcl-x_L·Bak, the ratio was 1 : 1 (eq.) and for the Bcl-x_L·Bad binding 1 : 6.6 (eq.). The experiments are described in detail in the next section.

Monitoring the Bcl-x_L·Bak and Bcl-x_L·Bad inhibition using small disruptors ABT737 and ABT263

We used native MS to directly monitor the inhibition of the Bcl-x_L·Bak and Bcl-x_L·Bad heterodimers in the presence of the small inhibitors ABT737 and ABT263. These compounds were shown to inhibit binding of peptide and induce apoptosis.[34]

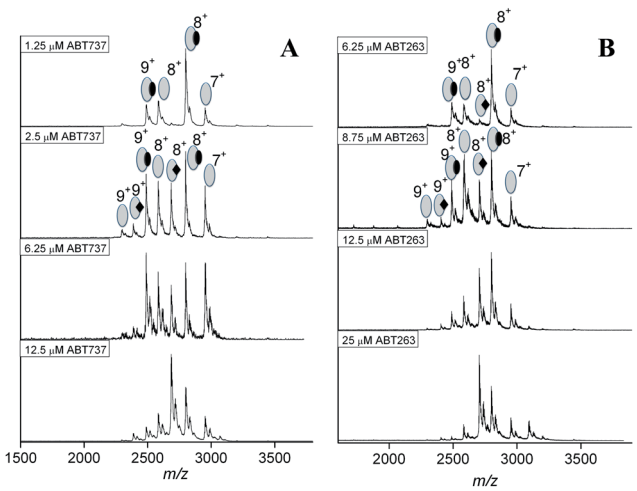

Fig. 4 NanoESI mass spectra of 3 μM Bcl-x_L in complex with 3 μM Bak (filled circle) in the presence of different concentrations of small disruptor (filled rhombus) (A) ABT737 and (B) ABT263. The heterodimer signal clearly decreases with increasing inhibitor concentration present in solution.

Experiments with the small disruptor ABT737 of the Bcl-x_L·Bak heterodimer were first carried out. In Fig. 4A the spectra of 3 μM Bcl-x_L in complex with 3 μM Bak (full complexation reached), in the presence of different ABT737 concentrations ranging from 1.25 to 12.5 μM are shown. With higher inhibitor concentration we can clearly monitor the increasing disruption of the Bcl-x_L·Bak interaction. Upon addition of the small inhibitor the disrupted Bcl-x_L·Bak complex generates additional peaks of the bare Bcl-x_L protein and a Bcl-x_L·ABT737 complex. This observation gives us additional information about the mechanism of binding of the ABT737, which in this case is competitive. The small disruptor ABT737 is able to displace the Bak derived peptide from the BH3 binding pocket of Bcl-x_L. No peaks where all three species form a complex were detected, which confirm our interpretation of a competitive mechanism. In a recent study it was described that ABT binds to the BH3 pocket of Bcl-x_L, breaking its hold on Bak.[29,34] At 12.5 μM ABT737 the major +8 peak is Bcl-x_L in complex with ABT737, only a minor undisrupted +8 heterodimer peak remains.

For the native MS measurements of the Bcl-x_L·Bak disruption in the presence of the small inhibitor ABT263, the same instrument conditions were used. In Fig. 4B the spectra of 3 μM Bcl-x_L in complex with 3 μM Bak and in the presence of ABT263 at different concentrations between 6.25 μM and 25 μM are shown. The mode of binding is, as in the previous case, competitive, although a significant difference in the inhibition of PPI compared to ABT737 was detected. In order to disrupt half of the heterodimer, 17.5 μM of ABT263 had to be present in solution. As shown in Fig. 5, 6.25 μM ABT737 disrupts three times more Bcl-x_L·Bak complex compared to ABT263 at the same concentration.

This observation lets us conclude that ABT263 is a less active inhibitor compared to ABT737. These data are consistent with those generated in a TR-FRET assay, which also indicate that

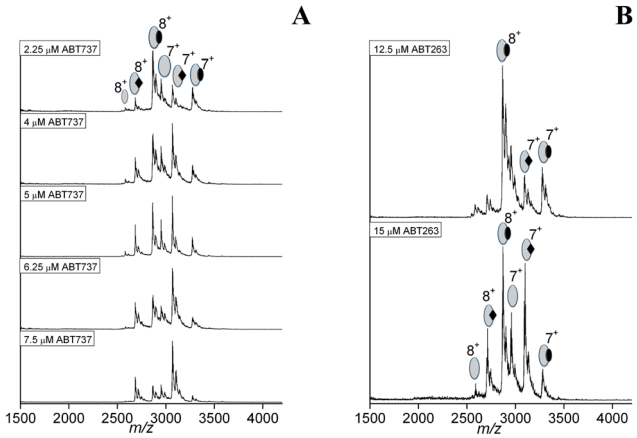

Fig. 5 NanoESI mass spectra of 3 μM Bcl-x_L in complex with 20 μM Bad (filled circle) in the presence of different concentrations of small disruptor (filled rhombus) (A) ABT737 and (B) ABT263.

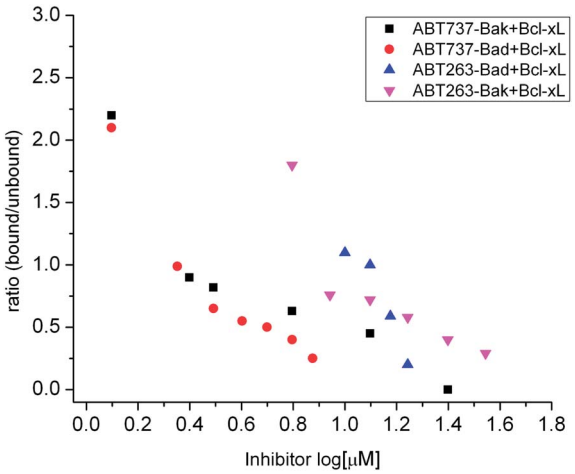

Fig. 6 Plotted ratios (bound heterodimers/unbound bare Bcl-x_L and Bcl-x_L·ABT737 complex) against the different inhibitor concentrations in order to dissociate the heterodimer.

ABT737 is more active than ABT263.[34] In addition, the *in vitro* efficacies of ABT737 and ABT263 were investigated in a recent study. The authors have shown that ABT737 is more active than ABT263 in inducing apoptosis in chronic lymphocytic leukemia (CCL) cells, because ABT263 was more strongly bound by albumin compared to ABT737, which accounted for the differential sensitivity of CLL cells.[45] However, the activities in our assay using purified protein are not affected by albumin binding.

In a second step, we also studied the influence of ABT737 and ABT263 on the Bcl-x_L·Bad interaction. For this the experiments with the small inhibitors with 3 μM Bcl-x_L in complex with 20 μM Bad were performed. Fig. 5 displays nanoESI spectra at different ABT737 and ABT263 concentrations. Again, with higher inhibitor concentration the stronger disruption of the Bcl-x_L·Bad interaction is detected. The disrupted Bcl-x_L·Bad complex dissociates into ions representing the bare Bcl-x_L protein and the Bcl-x_L·ABT737 or Bcl-x_L·ABT263 complexes. We found again that the ABT737 is more potent compared to ABT263 in preventing the heterodimerization between Bcl-x_L and Bad derived BH3 peptide in solution. To completely dissociate the dimerization, a 2.5 times higher concentration of ABT263 was required, corresponding to the 18 μM ABT263 and 7 μM ABT737 inhibitor concentrations.

The heterodimer ratios (Bcl-x_L·Bak/Bcl-x_L or Bcl-x_L·Bad/Bcl-x_L) upon addition of the total ABT263 and ABT737 concentration are plotted in Fig. 6. Compared to Bcl-x_L·Bak, no significant difference in the inhibitor efficiency is observed in preventing the Bcl-x_L·Bad interaction; ABT737 and ABT263 seem to have a very similar influence in disrupting both investigated heterodimers. For the Bcl-x_L·Bad disruption with ABT263, no significant difference in dissociation of the heterodimer with lower ABT263 concentration is observed. Therefore less data points are plotted compared to other three investigated systems. We could show that the native MS approach is suitable to directly monitor not only PPI inhibition, but also the relative binding strengths and the nature of binding.

Conclusions

In this study we investigated the inhibition of protein–protein interactions using nanoESI-MS. As a first system we investigated the dissociation of the trimeric TNF-alpha in the presence of the inhibitor SPD304. Ion mobility experiments were performed as well. The inhibitor promotes subunit disassembly of the trimeric form into monomers and dimers. Only one molecule inhibitor binds to the trimeric TNF-alpha. The SPD304-promoted dissociation into dimers ions must have been present in the sample prior to IMS-MS analysis, since the dimeric ions have their own characteristic drift time distributions, which are different from those of dimer ions originating in the gas phase due to CID.

As a second system we investigated the inhibition of the heterodimer formation of the survival protein Bcl-x_L and death-promoting regions of proteins Bak and Bad. Recently developed small-molecule inhibitors for the above-mentioned interaction, ABT737 and ABT263, were used to detect the disruption of the heterodimers. In the first step we determined the dissociation constants of the Bcl-x_L in complex with Bak or Bad derived peptide domain by applying a titration method. The ratio of the protein–peptide wherein the complex peak was generated was used for further experiments with small inhibitors. We found that ABT737 is a more active inhibitor compared to ABT263 in disrupting the heterodimerization between Bcl-x_L and Bak and also Bad derived BH3 peptide. The small disruptor ABT737 as well as ABT263 is able to displace the Bak and Bad derived peptide from the BH3 mainly hydrophobic pocket of the Bcl-x_L. This observation indicates a competitive mode of binding.

The nanoESI-based results for both investigated systems are in agreement with our biophysical methods in terms and can therefore be used as a suitable/appropriate technique for studying PPI inhibition. Due to the advantages of the nanoESI approach in terms of speed, absence of label and sensitivity, we believe that can be widely used for better understanding and

development of small inhibitors of PPIs. This method allows the monitoring of ligation states, provides information of mechanisms, on stoichiometry and relative binding potency.

Acknowledgements

This research was supported by the Research Executive Agency (REA) of the European Union under Grant Agreement number PITN-GA-2010-264772 (ITN CHEBANA). We thank Prof. Ho Sup Yoon (Nanyang Technological University, Singapore) for the Bcl-x_L plasmid. We would like to thank Michael Hell, ETH Zurich for helpful discussion.

References

1 M. R. Arkin and J. A. Wells, *Nat. Rev. Drug Discovery*, 2004, **3**, 301.
2 J. A. Wilson, *Chem. Soc. Rev.*, 2009, **38**, 3289.
3 E. Valkov, T. Sharpe, M. Marsh, S. Greive and M. Hyvönen, in *Fragment-Based Drug Discovery and X-Ray Crystallography*, Springer Berlin, Heidelberg, 2012, vol. 317.
4 N. Gasilova and A. Nazabal, in *Chemical Proteomics*, ed. G. Drewes and M. Bantscheff, Humana Press, 2012, vol. 803.
5 L. T. Vassilev, B. T. Vu, B. Graves, D. Carvajal, F. Podlaski, Z. Filipovic, N. Kong, U. Kammlott, C. Lukacs, C. Klein, N. Fotouhi and E. A. Liu, *Science*, 2004, **303**, 844.
6 E. N. Kitova, A. El-Hawiet, P. D. Schnier and J. S. Klassen, *J. Am. Soc. Mass Spectrom.*, 2012, **23**, 431.
7 H. J. Maple, R. A. Garlish, L. Rigau-Roca, J. Porter, I. Whitcombe, C. E. Prosser, J. Kennedy, A. J. Henry, R. J. Taylor, M. P. Crump and J. Crosby, *J. Med. Chem.*, 2012, **55**, 837.
8 M. A. Cooper, *Nat. Rev. Drug Discovery*, 2002, **1**, 515.
9 W. F. de Azevedo and R. Dias, *Curr. Drug Targets*, 2008, **9**, 1071.
10 B. Meyer and T. Peters, *Angew. Chem., Int. Ed.*, 2003, **42**, 864.
11 S. A. Hofstadler and K. A. Sannes-Lowery, *Nat. Rev. Drug Discovery*, 2006, **5**, 585.
12 J. M. Daniel, G. McCombie, S. Wendt and R. Zenobi, *J. Am. Soc. Mass Spectrom.*, 2003, **14**, 442.
13 A. Tjernberg, S. Carno, F. Oliv, K. Benkestock, P. O. Edlund, W. J. Griffiths and D. Hallen, *Anal. Chem.*, 2004, **76**, 4325.
14 M. V. Sharon and C. Robinson, *Curr. Proteomics*, 2011, **8**, 47.
15 K. Lorenzen and E. V. Duijn, *Curr. Protoc. Protein Sci.*, John Wiley & Sons, Inc., 2001, pp. 17.12.1–17.12.17.
16 K. Breuker and F. W. McLafferty, *Proc. Natl. Acad. Sci. U. S. A.*, 2008, **105**, 18145.
17 S. Zhang, C. K. Van Pelt and W. D. Wilson, *Anal. Chem.*, 2003, **75**, 3010.
18 J. Zhang, G. McCombie, C. Guenat and R. Knochenmuss, *Drug Discovery Today*, 2005, **10**, 635.
19 G. J. Deng and G. Sanyal, *J. Pharm. Biomed. Anal.*, 2006, **40**, 528.
20 J. A. Loo, *Mass Spectrom. Rev.*, 1997, **16**, 1.
21 J. A. Loo, P. Hu, P. McConnell and W. T. Mueller, *J. Am. Soc. Mass Spectrom.*, 1997, **8**, 234.
22 C. Atmanene, S. Petiot-Bécard, D. Zeyer, A. Van Dorsselaer, V. Vivat Hannah and S. Sanglier-Cianfèrani, *Anal. Chem.*, 2012, **84**, 4703.
23 W. Davidson, J. Hopkins, D. Jeanfavre, K. Barney, T. Kelly and C. Grygon, *J. Am. Soc. Mass Spectrom.*, 2003, **14**, 8.
24 S. Niu, J. N. Rabuck and B. T. Ruotolo, *Curr. Opin. Cell Biol.*, 2013, **17**, 809.
25 Z. Hall and C. V. Robinson, *J. Am. Soc. Mass Spectrom.*, 2012, **23**, 1161.
26 A. Konijnenberg, A. Butterer and F. Sobott, *Biochim. Biophys. Acta, Proteins Proteomics*, 2013, **1834**, 1239.
27 M. M. He, A. S. Smith, J. D. Oslob, W. M. Flanagan, A. C. Braisted, A. Whitty, M. T. Cancilla, J. Wang, A. A. Lugovskoy, J. C. Yoburn, A. D. Fung, G. Farrington, J. K. Eldredge, E. S. Day, L. A. Cruz, T. G. Cachero, S. K. Miller, J. E. Friedman, I. C. Choong and B. C. Cunningham, *Science*, 2005, **310**, 1022.
28 M. Gräber, M. Hell, C. Gröst, A. Friberg, B. Sperl, M. Sattler and T. Berg, *Angew. Chem., Int. Ed.*, 2013, **52**, 4487.
29 T. Oltersdorf, S. W. Elmore, A. R. Shoemaker, R. C. Armstrong, D. J. Augeri, B. A. Belli, M. Bruncko, T. L. Deckwerth, J. Dinges, P. J. Hajduk, M. K. Joseph, S. Kitada, S. J. Korsmeyer, A. R. Kunzer, A. Letai, C. Li, M. J. Mitten, D. G. Nettesheim, S. Ng, P. M. Nimmer, J. M. O'Connor, A. Oleksijew, A. M. Petros, J. C. Reed, W. Shen, S. K. Tahir, C. B. Thompson, K. J. Tomaselli, B. Wang, M. D. Wendt, H. Zhang, S. W. Fesik and S. H. Rosenberg, *Nature*, 2005, **435**, 677.
30 H. Zhang, P. Nimmer, S. H. Rosenberg, S.-C. Ng and M. Joseph, *Anal. Biochem.*, 2002, **307**, 70.
31 A. M. Petros, A. Medek, D. G. Nettesheim, D. H. Kim, H. S. Yoon, K. Swift, E. D. Matayoshi, T. Oltersdorf and S. W. Fesik, *Proc. Natl. Acad. Sci. U. S. A.*, 2001, **98**, 3012.
32 M. Sattler, H. Liang, D. Nettesheim, R. P. Meadows, J. E. Harlan, M. Eberstadt, H. S. Yoon, S. B. Shuker, B. S. Chang, A. J. Minn, C. B. Thompson and S. W. Fesik, *Science*, 1997, **275**, 983.
33 S. W. Muchmore, M. Sattler, H. Liang, R. P. Meadows, J. E. Harlan, H. S. Yoon, D. Nettesheim, B. S. Chang, C. B. Thompson, S.-L. Wong, S.-C. Ng and S. W. Fesik, *Nature*, 1996, **381**, 335.
34 C. Tse, A. R. Shoemaker, J. Adickes, M. G. Anderson, J. Chen, S. Jin, E. F. Johnson, K. C. Marsh, M. J. Mitten, P. Nimmer, L. Roberts, S. K. Tahir, Y. Xiao, X. Yang, H. Zhang, S. Fesik, S. H. Rosenberg and S. W. Elmore, *Cancer Res.*, 2008, **68**, 3421.
35 F. Curnis and A. Corti, *Methods Mol. Med.*, 2004, **98**, 9.
36 H. Rogniaux, S. Sanglier, K. Strupat, S. Azza, O. Roitel, V. Ball, D. Tritsch, G. Branlant and A. Van Dorsselaer, *Anal. Biochem.*, 2001, **291**, 48.
37 S. K. Chowdhury, V. Katta and B. T. Chait, *J. Am. Chem. Soc.*, 1990, **112**, 9012.
38 V. Katta and B. T. Chait, *J. Am. Chem. Soc.*, 1991, **113**, 8534.
39 D. Cubrilovic and R. Zenobi, *Anal. Chem.*, 2013, **85**, 2724.
40 J. L. Benesch and C. V. Robinson, *Curr. Opin. Struct. Biol.*, 2006, **16**, 245.

41 J. D. Bryngelson, J. N. Onuchic, N. D. Socci and P. G. Wolynes, *Proteins: Struct., Funct., Bioinf.*, 1995, **21**, 167.
42 L. O. Narhi, J. S. Philo, T. Li, M. Zhang, B. Samal and T. Arakawa, *Biochemistry*, 1996, **35**, 11447.
43 M. Jecklin, D. Touboul, C. D. Bovet, A. Wortmann and R. Zenobi, *J. Am. Soc. Mass Spectrom.*, 2008, **19**, 332.
44 A. M. Petros, D. G. Nettesheim, Y. Wang, E. T. Olejniczak, R. P. Meadows, J. Mack, K. Swift, E. D. Matayoshi, H. Zhang, S. W. Fesik and C. B. Thompson, *Protein Sci.*, 2000, **9**, 2528.
45 M. Vogler, S. D. Furdas, M. Jung, T. Kuwana, M. J. S. Dyer and G. M. Cohen, *Clin. Cancer Res.*, 2010, **16**, 4217.